Photocycle Dynamics and Vibrational Spectroscopy of the E46Q Mutant of Photoactive Yellow Protein†

Yidong Zhou,‡,|| Laszlo Ujj,‡,⊥ T. E. Meyer,*,§ M. A. Cusanovich,*,§ and G. H. Atkinson*,‡

Department of Chemistry and Optical Science Center and Department of Biochemistry, University of Arizona, Tucson, Arizona 85721

Received: December 22, 2000

The dynamics over the initial 100 ns (3 ps time resolution) of the room-temperature photocycle of the E46Q mutant of photoactive yellow protein (PYP^{E46Q}) are measured using picosecond transient absorption (PTA) spectroscopy. Three intermediates, I_0^{E46Q}, $I_0^{‡E46Q}$, and I_1^{E46Q}, are observed in the room-temperature PYP^{E46Q} photocycle. Although their respective formation and decay rates differ, I_0^{E46Q}, $I_0^{‡E46Q}$, and I_1^{E46Q} correspond to analogous intermediates (i.e., I_0, $I_0^‡$, and I_1) observed by PTA in the room-temperature photocycle of the wild type (WT) photoactive yellow protein (PYP). These PTA data show that the replacement of glutamic acid 46 with glutamine influences the kinetic properties of the PYP photocycle, but does not alter the general photochemical mechanism itself. The influence of the E46Q mutation on the PYP chromophore can be independently obtained by measuring changes in the vibrational degrees of freedom of ground-state PYP and PYP^{E46Q}. Vibrational spectra (1100−1700 cm^{-1}) of both PYP and PYP^{E46Q} are measured under the same experimental conditions (i.e., $\omega_1 = 490$ nm and $\omega_s = 518-535$ nm) using picosecond resonance coherent anti-Stokes Raman scattering (PR/CARS). Although the 14 vibrational bands observed in the PR/CARS spectrum of PYP^{E46Q} are generally analogous to those found in the PR/CARS spectrum of PYP, detailed comparisons reveal significant differences in both the positions and relative intensities of vibrational bands assigned to the phenolate part of the cinnamyl chromophore. These PR/CARS results demonstrate that while the chromophore within both PYP and PYP^{E46Q} have similar vibrational degrees of freedom, the E46Q mutation selectively alters the structure of the phenolate ring, apparently through differences in the hydrogen bonding network involving glutamic acid 46 and the negatively charged oxygen in the phenolate ring. When considered together, the changes in the kinetic rate constants for the photocycle (PTA data) and in the vibrational spectra (PR/CARS data) caused by the E46Q mutation suggest that the I_0 and $I_0^‡$ intermediates involve structural and/or electronic energy changes localized on the phenolate ring of the PYP chromophore.

Introduction

The photoactive yellow protein (PYP) from *Ectothiorhodospira halophila* is a small (14 kDa) water-soluble, cytoplasmic protein which exhibits a photocycle containing intermediates with lifetimes spanning the 100 fs to seconds time interval.[1,2] Room-temperature PYP, absorbing in the blue (Figure 1), has a photocycle comprised of at least four intermediates (I_0, $I_0^‡$, I_1, and I_2), all of which have been identified by transient absorption spectroscopy using different time resolution.[3] PYP is thought to function as a blue-light photoreceptor which activates negative phototaxis,[4] although a PYP−phytochrome hybrid protein is involved in the regulation of chalcone synthesis in *Rhodospirillum centenum*.[5]

The chromophoric group in PYP was identified by a combination of NMR spectroscopy and capillary electrophoresis[6] and by a combination of mass spectroscopy and X-ray crystallography[7,8] as a 4-hydroxycinnamyl cysteine thioester (Figure 2). The structure of ground-state PYP is known to high resolution (1.4 Å).[8] In addition, the crystal structure of some intermediate(s) in the photocycle, presumably both I_2 and I_1, with time resolutions ranging from 1 ns to a few ms[9−11] have been determined for a variety of conditions (e.g., sample temperatures from 163 to 287 K). These results suggest that

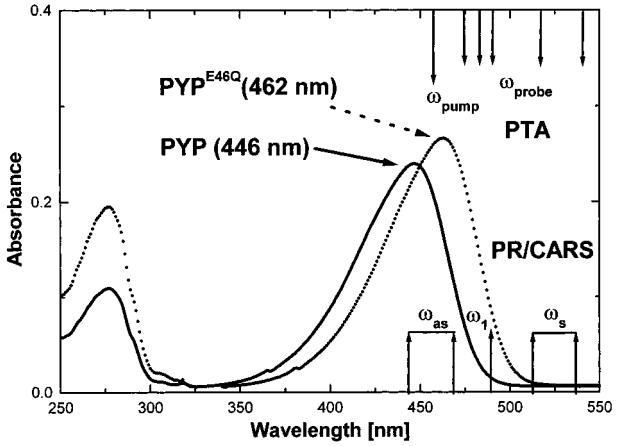

Figure 1. Absorption spectra of photoactive yellow protein (PYP, 446 nm maximum, solid line) and of its E46Q mutant (PYP^{E46Q}, 462 nm maximum, dotted line) at pH = 7.0. The excitation (460 nm) and probe (475, 483, 491, 519, and 544 nm) wavelengths used for picosecond transient absorption (PTA) measurements are shown schematically at the top. The probe ($\omega_1 = 490$ nm) and probe ($\omega_s = 518-535$ nm) wavelengths used for the picosecond resonance coherent anti-Stokes Raman spectroscopy (PR/CARS) are shown at the bottom together with the spectral region where the ω_{as} (440−465 nm) signal appears.

† Part of the special issue "Edward W. Schlag Festschrift".

* To whom correspondence should be addressed.
‡ Department of Chemistry and Optical Science Center.
§ Department of Biochemistry.
|| Current address: Lightwave Electronics, Mountain View, CA 94043.
⊥ Current address: Department of Physics, University of Western Florida, Pensacola, FL 32514.

10.1021/jp004575u CCC: $20.00
Published on Web 03/23/2001

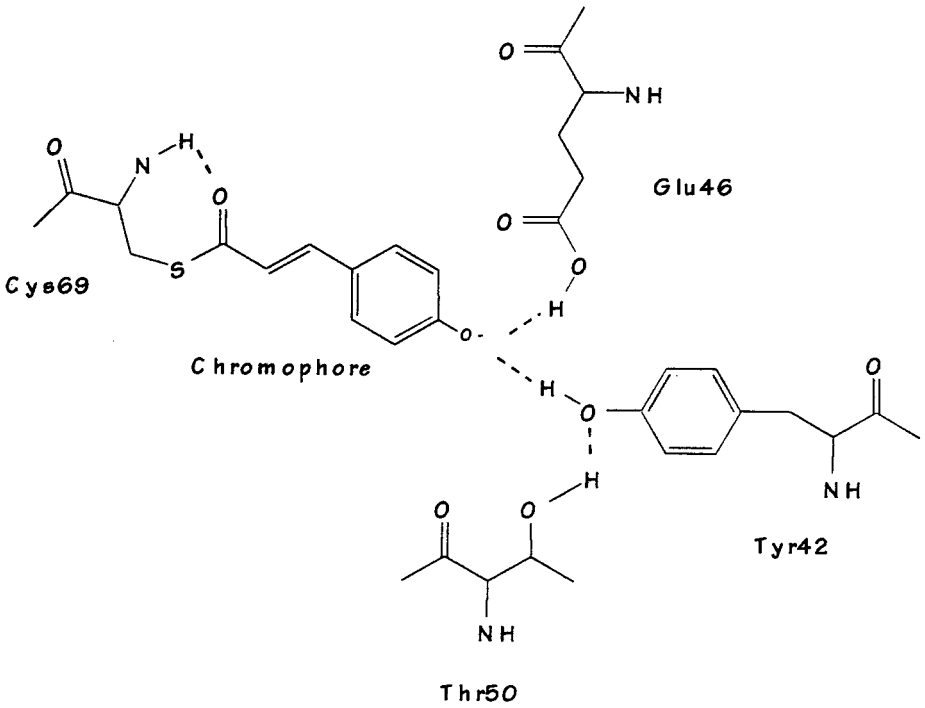

Figure 2. Schematic structure of the chromophore in PYP which is involved in a hydrogen bonding network connecting the negatively charged phenolate oxygen of the chromophore to nearby active-site amino acid residues in the ground state of PYP.

the 4-hydroxycinnamyl cysteine chromophore isomerizes by rotating its thioester linkage to the protein, a mechanism that would avoid large-scale movement of the PYP aromatic ring during the initial stages of the photocycle.[10,11] It appears that the trans−cis isomerization is followed by protein-linked structural changes that alter the hydrogen bonding patterns of the chromophore, resulting in a change of both the chromophore shape and its exposure to the solvent, thereby altering the electrostatic surface potential.[9] Thus, the negatively charged oxygen in the phenolate part of the protein−chromophore binding pocket and the relative positions of the hydrogen-binding partners (E46, Y42, and T50) within the hydrophobic binding pocket are affected.[9−12]

The structural mechanism operative in the room-temperature PYP photocycle is yet to be quantitatively resolved. Even the specific relationship(s) between the low-temperature and room-temperature structural data reported to date has not been clearly established.[9−11] Following the excitation of the ground-state of PYP (absorption spectrum in Figure 1), data derived from transient absorption spectroscopy have shown that the room-temperature PYP photocycle proceeds mechanistically: I_0 is formed from the excited electronic state populated by optical excitation of PYP (PYP^*) in <3 ps and decays to $I_0^‡$ in 220 ps,[3] $I_0^‡$ decays to I_1 with a 3 ns time constant, I_1 decays to I_2 with a 200 μs time constant, and I_2 re-forms ground-state PYP in ∼140 ms to complete the photocycle. Strong pH dependencies are observed in the rate constants comprising the later stages of the respective PYP[12−14] and PYP^{E46Q} photocycles[15] and are thought to reflect changes in protonation state, especially for the chromophoric hydroxyl and the E46 carboxyl.

The absorption spectrum assignable to each intermediate shows that both I_0 and $I_0^‡$ have red-shifted absorption maxima relative to PYP (the absorption spectrum of $I_0^‡$ is slightly red-shifted from I_0 and has a distinct reduction in intensity[3]), while I_1 is blue-shifted relative to both I_0 and $I_0^‡$ while remaining red-shifted relative to PYP.[3] The absorption maximum of I_2 (∼350 nm) is blue-shifted relative to the absorption spectrum of PYP.[16,17]

The extensive study of Glu at position 46 has revealed its role in forming important hydrogen bonds (Figure 2) and as the proton donor to the chromophore during the photocycle.[12,15] The E46Q mutation results in a shift in the ground-state absorption maxima from 446 to 462 nm and a 700-fold increase in the rate of recovery to the ground state between pHs 5 and 10.[15] It has been proposed that substitution of Gln for Glu at position 46 results in the hydrogen atom in the O···H···N hydrogen bond (as opposed to a O···H···O bond in wild type) being positioned further from the chromophore in the mutant.[15] Thus, the change in the hydrogen bond strength is believed to be responsible, at least in part, for the kinetic and spectral consequences of a mutation by an increase in the negative charge on chromophore.[15]

Although the X-ray data show that isomerization of the chromophore occurs around the C_7═C_8 bond during the PYP photocycle,[9−11] the structural changes comprising each step of the PYP mechanism remain unknown. Moreover, the exact point during the photocycle at which the structural changes occur is also not known. Of particular importance in the structural mechanism are the contributions, if any, of the amino acids comprising the binding pocket and of the hydrogen bonding network formed by the 4-hydroxycinnamyl phenolate and the adjacent amino acids (Figure 2). Site-directed mutagenesis is used in this study to selectively alter the amino acid composition of the binding pocket (i.e., PYP^{E46Q}), thereby altering the hydrogen bonding network. This work focuses on determining how this change in the hydrogen-bonding network alters the vibrational spectrum of the PYP chromophore and, thereby, how it affects the structure of the PYP chromophore.

The photocycle dynamics of PYP^{E46Q} are measured by picosecond transient absorption (PTA) spectroscopy over the time interval from −300 ps to 104 ns. The ground-state vibrational spectra of both PYP and PYP^{E46Q} are recorded by picosecond resonance coherent anti-Stokes Raman spectroscopy (PR/CARS) under the same experimental conditions in order to facilitate a direct comparison of their respective vibrational

band positions and relative intensities. The significant differences observed in both the PTA and PR/CARS results between PYP and PYP^{E46Q} demonstrate that the alteration of the protein environment (hydrogen bonding) caused by the E46Q mutation (i) alters the rates by which intermediates are formed and decay during the initial 100 ns of the photocycle and (ii) selectively changes the vibrational structure of the chromophoric phenolate.

Experimental Section

A. Materials. The PYP protein, produced in *Escherichia coli* (*E. coli*), is purified according to established methods.[18] The sample used in the PTA and PR/CARS measurements consists of 15 mL of a 3.5 OD/cm solution in 20 mM Tris-Cl buffer at pH 7.0. The PYP and PYP^{E46Q} samples examined have an absorption ratio for the protein (280 nm) to the chromophore (447 or 462 nm) of ~0.5 and ~0.67, respectively. All experiments are performed at 17 °C.

B. Instrumentation and Procedures. The instrumentation used to record PTA and PR/CARS consists of two pulsed (ps) dye lasers synchronously pumped by the third-harmonic output of a continuous wave (cw), mode-locked Nd:YAG laser. Since this system is described in detail elsewhere,[19] only a brief description of the fundamental components is presented here.

The 1064 nm output (80 ps pulses at 76 MHz repetition rate) of a cw, mode-locked Nd:YAG laser (Coherent, Antares 76) is used to generate third-harmonic radiation (355 nm) from a BBO crystal which is used to pump two, independently controlled dye lasers (Coherent, model 701-3). A combination of polarizing beam splitters and half-wave plates is used to adjust the output power of each dye laser to an appropriate level (0.6−1 W). Each dye laser is operated with a cavity dumper (Coherent, models 7210 and 7220) which is synchronized to the 76 MHz repetition rate of the mode locker used with the Nd:YAG pump laser. The entire laser system is operated at a 400 kHz repetition rate in order to match the flow properties of the liquid sample jet.[20]

The narrow-band (<2 cm^{-1}, full width at half-maximum (fwhm)) dye laser is operated at 490 nm (ω_1) with a coumarin 480 dye (~20 nJ/pulse) using an intracavity, three-plate birefringent filter. The temporal autocorrelation width (fwhm) of the laser pulses, as measured by a rapidly scanned autocorrelator, is ~7.5 ps. If a Gaussian pulse shape is assumed, the corresponding pulse width is ~5.5 ps.

The generation of a broad wavelength (e.g., 600 cm^{-1}), picosecond pulse is achieved with a synchronously pumped, cw mode-locked dye laser by removing the intracavity birefringent filter from the laser cavity. When properly phase matched with the ω_1 beam in the sample, the resultant 600 cm^{-1} (fwhm) output (ω_s) from the dye laser (operated with coumarin 503 dye) is used to generate CARS signals over the entire 1100−1700 cm^{-1} range. The instrumental conditions are selected to obtain the maximum output energy (~15 nJ/pulse) and the shortest pulse width (~15 ps). In PTA experiments, an intracavity birefringent filter is inserted in the ω_s laser to narrow the spectral output and shorten the pulse width (~8 ps).

The PTA traces, utilizing probe laser pulses at five selected wavelengths (475, 483, 491, 519, and 544 nm) are recorded continuously as a function of delay time in two sets of experiments spanning the −100 ps to +500 ps interval and the −300 ps to +4.5 ns interval. Operation of dye lasers at these wavelengths results in different cross-correlation times (CCT): 9 ps at 491 nm, 30 ps at 475 and 483 nm, and 8 ps at 519 and 544 nm. These CCT values permit time constants as short as 3 ps to be confidently extracted through quantitative, global fits encompassing all three sets of PTA data. Time delays of 26, 52, 78, and 104 ns are recorded discretely by using electronic delays afforded by the timing sequence of the respective cavity dumpers.

TABLE 1: Time Constants for the Formation (τ_f) of Intermediates Comprising the Room-Temperature PYP Photocycle (PYP + $h\nu$ → PYP* → I_0 → $I_0^{\ddagger}$ → I_1 → I_2 → PYP) and Its Mutant PYP^{E46Q}

PYP	τ_f	PYP^{E46Q}	τ_f
I_0	<3 ps [3]	I_0^{E46Q}	< 3 ps [a]
$I_0^{\ddagger}$	220 ps [3]	$I_0^{\ddagger E46Q}$	14 ± 2 ps [a]
I_1	3.0 ns [3]	I_1^{E46Q}	1.7 ± 0.2 ns [a]
I_2	220 μs [13]	I_2^{E46Q}	10−40 μs [b]
PYP	140 ms [13]	PYP^{E46Q}	2.5 ms − 2 s [b]

[a] This work. [b] pH dependent.[15]

PR/CARS signals are generated simultaneously from two separate sample compartments, reference and protein (native or mutant).[19] The reference compartment is a capillary containing a static water sample placed next to the nozzle (400 μm) through which the protein sample flows. This configuration permits the simultaneous measurement of the nonresonant background from the water/buffer and the PR/CARS signal from the protein, thereby normalizing any fluctuations in the instrumental response. Both types of PR/CARS signals are spectrally dispersed with a monochromator (SPEX Triplemate) and reflected onto the surface of a liquid nitrogen-cooled, two-dimensional (256 × 1024 pixel) CCD detector (EG&G, model 1024) which records the signals from both the flowing protein (mutant) and reference sample.

PR/CARS spectra are fitted with a third-order, nonlinear susceptibility ($\chi^{(3)}$) model function described in detail elsewhere.[19] Such a $\chi^{(3)}$ fitting procedure provides quantitative data characterizing the vibrational spectra in terms of amplitude, bandwidth, band origin position, and relative electronic phase factors.[19] The availability of a variety of vibrational bands in these PR/CARS spectra makes it feasible to derive vibrational normal mode assignments.

Results

A. PYP^{E46Q} Photocycle in the 3 ps to 100 ns Regime. Although transient absorption data recorded over periods of >1 μs[15] have shown PYP^{E46Q} to have a photocycle which re-forms ground-state PYP^{E46Q} within a range of 2.5 ms to 2.0 s (pH dependent[15]), the earlier stages (1 ps to 100 ns) of the photocycle have until recently not been studied.

In a recent publication, kinetic rates for the $I_0^{E46Q} \rightarrow I_0^{\ddagger E46Q}$ (8 ps) and $I_0^{\ddagger E46Q} \rightarrow I_1$ (0.7 ns) were reported.[20] These values are respectively about half of the 14 ± 2 ps and 1.7 ± 0.2 ns values reported here (Table 1). These differences are attributable to differences in the signal-to-noise ratios available in these two studies (Figures 2−4 in ref 20 and Figures 3 and 4 [this work]). Good agreement is found in the formation rates of I_0^{E46Q} (2.3 ps[20] versus <3.0 ps [this work]). It should be noted, however, that the instrumentation in this work as well as the precision of these transient absorption (PTA) measurements, are quite different from those reported by Devanathan, et al.[20] Given the differences in time domains examined, and *S*/*N* in the kinetic traces, the general agreement between the kinetic parameters reported in the two studies is reasonable, although it is evident that the improved *S*/*N* in the data presented here provides the basis for the significantly more precise time constants (Table 1). Irrespective of the foregoing, it was independently necessary to measure PYP^{E46Q} kinetics under conditions (e.g., excitation and probe wavelengths) relevant to the measurement of vibra-

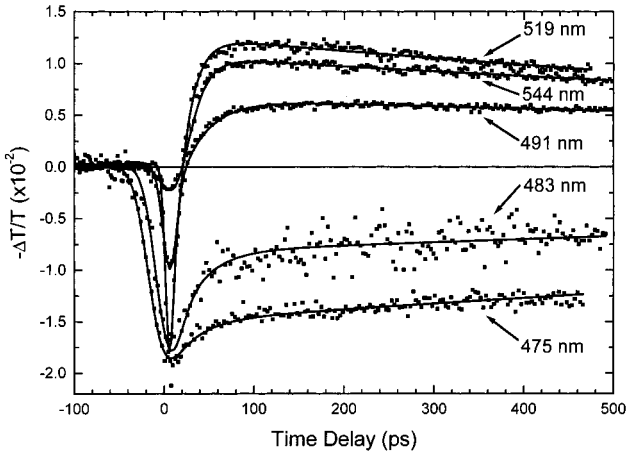

Figure 3. PTA traces (solid lines) for PYP^{E46Q} obtained for five probe wavelengths at 475, 483, 491, 519, and 544 nm over the −100 to +500 ps time period (3 ps time resolution). Solid lines correspond to global fits of the PTA data.

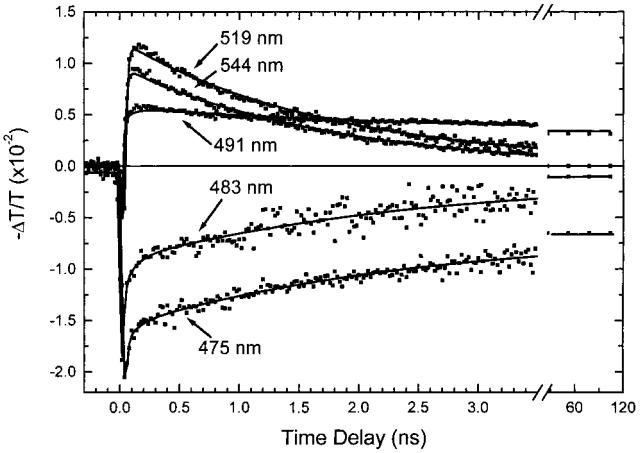

Figure 4. PTA traces (dotted lines) for PYP^{E46Q} obtained for five probe wavelengths at 475, 483, 491, 519, and 544 nm over the −300 ps to +4.5 ns (20 ps time resolution) time period. PTA data recorded at four discrete time delays (26, 52, 78, and 104 ns) are shown at the right. Solid lines correspond to global fits of the PTA data.

tional spectra (described below) in order to facilitate accurate comparisons between the kinetic properties of the PYP^{E46Q} photocycle and the vibrational data from PYP and PYP^{E46Q}.

The PTA data presented here, recorded from −300 ps to +104 ns and at probe wavelengths of 475, 483, 491, 519, and 544 nm (Figures 3 and 4), are consistent with the appearance of three intermediates: I_0^{E46Q}, $I_0^{\ddagger E46Q}$, and I_1^{E46Q}. These PTA data are recorded continuously using 3 ps steps in the −100 ps to +500 ps interval (Figure 3) and with 20 ps steps in the −300 ps to +4.5 ns interval (Figure 4). In addition, four separate transient absorption measurements are made at all five probe wavelengths using electronic time delays of 26, 52, 78, and 104 ns (Figure 4). In all these cases, 5 ps pulses are used to excite PYP^{E46Q} (avoiding secondary photochemistry on longer time scales) and measurement conditions are selected which quantitatively preserve the timing and intensity relationships, thereby making direct comparisons of different PTA signals feasible.

The global fit analysis of these PTA traces utilizes a multiexponential function (solid line, Figures 3 and 4) to obtain formation and decay time constants[19] (Table 1). The resultant kinetic fits demonstrate that two distinct photochemical intermediates are present: I_0^{E46Q} appearing with a <3 ps time constant and decaying with a 14 ± 2 ps time constant and $I_0^{\ddagger E46Q}$ appearing with the 14 ± 2 ps time constant and decaying with a 1.7 ± 0.2 ns time constant. The $I_0^{\ddagger E46Q}$ intermediate is also distinguishable by its decreasing absorptivity at 491, 519, and 544 nm relative to I_0^{E46Q} over the 20−500 ps time range (Figure 3). The formation of I_1^{E46Q} following the decay of $I_0^{\ddagger E46Q}$ is also observed. The kinetic analysis of these PTA data does not show any change in the I_1^{E46Q} concentration over the 26−100 ns time period (Figure 4).

Stimulated emission, as observed with PYP,[3] may also contribute to the observed PTA data during the time interval when the probe and pump pulses overlap (<5 ps), but since the ground-state PYP^{E46Q} absorption spectrum overlaps significantly with all five probe wavelengths used here, no stimulated emission signals are identified in these data.

The appearance of I_0^{E46Q}, $I_0^{\ddagger E46Q}$, and I_1^{E46Q}, together with their respective formation and decay rate constants, generally correlates well with those observed in PYP (Table 1). The differences in the kinetics, however, are significant. Relative to the PYP photocycle, the transformation rate of I_0^{E46Q} into $I_0^{\ddagger E46Q}$ increases by a factor of >10, while the transformation rate of $I_0^{\ddagger E46Q}$ to I_1^{E46Q} increases by approximately a factor of 2. The time resolution of these PTA measurements permits only an upper limit to be placed on the formation rate of I_0^{E46Q} following ground-state excitation. Thus, the PYP photocycle dynamics involving I_0, $I_0^{\ddagger}$, and I_1 are influenced by the Glu46/Gln mutation and presumedly through the alteration of the hydrogen bonding network involving the cinnamyl phenolate.

B. Transient Absorption Spectra of I_0^{E46Q} and $I_0^{\ddagger E46Q}$. The relative intensities of these PTA data at given probe wavelengths and for a specific time interval provide insight into the relative wavelength positions of the respective absorption spectra of I_0^{E46Q}, $I_0^{\ddagger E46Q}$, and I_1^{E46Q}.

(1) During the initial 30-ps time interval when I_0^{E46Q} is present (Figure 4), the increase (relative to 0.00, Figure 3) of sample absorbance (-ΔT/T) at 491, 519, and 544 nm, together with its decrease at 483 and 475 nm, show that the absorption spectrum of I_0^{E46Q} is red-shifted relative to that of PYP^{E46Q} (Figure 1). These absorption properties for I_0^{E46Q} are similar to those of I_0 in the PYP photocycle.[3]

(2) During the 500 ps to 4 ns interval when $I_0^{\ddagger E46Q}$ is present (Figures 3 and 4), the sample absorbances at 491, 519, and 544 nm versus those at 483 and 475 nm respectively decreases or increase toward a −ΔT/T value of 0.0. These observations indicate that the intensity of the absorption spectrum assignable to $I_0^{\ddagger E46Q}$ decreases relative to that of I_0, but remains red-shifted relative to the PYP^{E46Q} absorption spectrum. These absorption properties for $I_0^{\ddagger E46Q}$ are similar to those of $I_0^{\ddagger}$ in the PYP photocycle[3]. A distinct wavelength shift in the absorption spectra of I_0^{E46Q} and $I_0^{\ddagger E46Q}$ would be manifested as differences between the rate at which −ΔT/T changes as a function of probe wavelength in these PTA data. The PTA data recorded here are not sufficiently precise to resolve this point. It is evident from these data, however, that the 491 nm trace crosses those for 519 and 544 nm at a time delay of about 1.2 ns (Figure 4), thereby indicating that the isosbestic point for I_0^{E46Q} and $I_0^{\ddagger E46Q}$ lies between 491 and 519 nm.

(3) During the 26−104 ns time interval when I_1^{E46Q} is present (Figures 3 and 4), the decrease (relative to the 3.5 ns signal) of sample absorbance (−ΔT/T) at 491, 519, and 544 nm together with its increase (relative to the 3.5 ns signal) at 483 and 475 nm, show that the absorption spectrum of I_1^{E46Q} is blue-shifted relative to that of $I_0^{\ddagger E46Q}$. The observation (Figure 4) that the PTA signals for the 491, 483, and 475 nm probe wavelengths all remain different from a −ΔT/T = 0.00 (the 519 and 544 nm traces decay to 0.00 before 26 ns, Figure 4) indicates that

TABLE 2: Vibrational Bands Observed at Different ω_1 Wavelengths for PYP Sample and PYP^{E46Q}

PYP					PYP^{E46Q}
RR[a] (cm^{-1})	vib mode assignment	PR/CARS[b] (cm^{-1})			PR/CARS[b] (cm^{-1})
ω_{excit} = 413 nm		ω_1 = 441 nm [c]	ω_1 = 470 nm [d]	ω_1 = 490 nm [e]	ω_1 = 490 nm [e]
1165	Y9a[f]	1162	1162	1161	1154
			1241	1243	1243
1288	CC(−S−)=O	1286	1285	1286	1285
		1307	1306	1306	1306
				1320	1321
		1339	1341	1343	1344
			1387		
1439	Y19b[f]	1437	1438	1439	1441
		1448	1449	1447	
1498	Y19a[f]	1488	1489	1488	1485
				1505	1507
1534	Y8a[f]	1532	1531	1532	1529
1558	Y8b[f]	1556	1557	1556	1552
			1590		1581
				1597	1598
1633	C=C		1626	1626	1626

[a] Resonance Raman.[25] [b] Picosecond resonance coherent anti-Stokes Raman spectroscopy, this work. [c] ω_s at 463−477 nm. [d] ω_s at 496−511 nm. [e] ω_s at 518−535 nm. [f] Tyrosine modes, see Table 4.

I_1^{E46Q} has an absorption spectrum that is red-shifted relative to that of PYP^{E46Q} (similar to the I_1 spectrum in the PYP photocycle[3]). These PTA data also show that the isosbestic point for I_1^{E46Q} and PYP^{E46Q} lies between 491 and 483 nm.

Since all of these spectral characteristics are analogous to those observed in PYP, it appears that the absorption spectra of I_0^{E46Q}, $I_0^{\ddagger E46Q}$, and I_1^{E46Q} are generally similar to those reported previously for I_0, $I_0\ddagger$, and I_1.[3,20]

C. Vibrational Spectrum of PYP^{E46Q}. The vibrational spectrum of PYP^{E46Q} is measured by PR/CARS in order to more fully characterize the effect of the Glu46/Gln mutation on the ground-state structure of the cinnamyl chromophore in PYP. Previous CARS studies have shown that structural changes are reflected in the vibrational spectrum of the chromophoric group from which resonantly enhanced Raman scattering is generated (i.e., from the absorption spectrum with which ω_1 and ω_s spectrally overlap).[21] PR/CARS data also have been shown to be exceptionally sensitive to changes in the structure of a chromophoric group within a protein,[22,23] including those attributable to changes in the surrounding amino acid environment comprising the binding pocket. The specific influence of the amino acids comprising the binding pocket in PYP is examined here, presumably since the hydrogen bonding network interacting with the negatively charged phenolate ring oxygen is perturbed by the E46Q mutation.

1. Resonance Enhancement and θ Values. The ω_1 and ω_s values used in the PR/CARS measurements described here are selected primarily to maximize the resonantly enhanced CARS signals from the cinnamyl chromophores in PYP and PYP^{E46Q}. Since the absorption maxima of PYP and PYP^{E46Q} at pH 7.0 are shifted by ∼16 nm (Figure 1), a given set of ω_1 and ω_s (Figure 1) values generates different degrees of resonantly enhanced CARS scattering (ω_{as}) from PYP and PYP^{E46Q}. To facilitate comparisons, the PR/CARS spectrum of PYP is recorded with the same ω_1 and ω_s values (490 nm and 518−535 nm, respectively) as those used for PYP^{E46Q} (Figure 1), *vide infra*. The pulse energy at ω_1 is selected to be low enough to avoid initiating the photocycle in either PYP or PYP^{E46Q}.

In general, the band origin positions of features in the PR/CARS spectrum of PYP generated with 490 nm excitation agree well with those observed using other excitation wavelengths

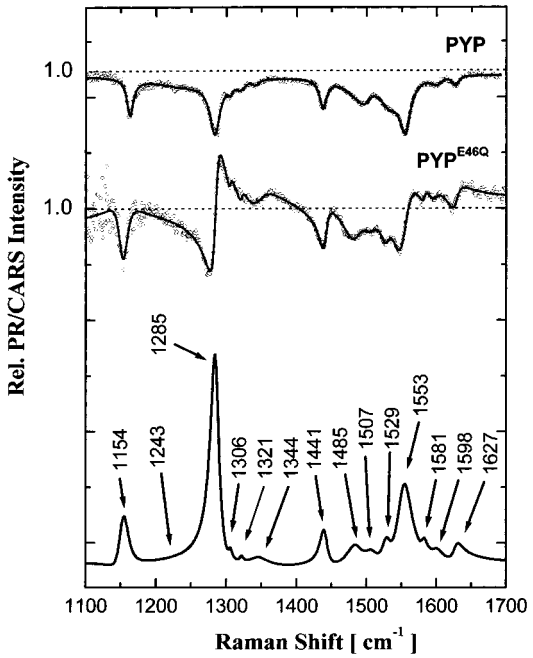

Figure 5. (Top) PR/CARS spectrum of PYP over the 1100−1700 cm^{-1} region. The $\chi^{(3)}$-fit function to these PR/CARS data is shown as a solid line. (Middle) PR/CARS spectra of PYP^{E46Q} over the 1100−1700 cm^{-1} region. The $\chi^{(3)}$-fit function is shown as a solid line. The horizontal, dashed lines in both PR/CARS spectra represent the nonresonant CARS background signal from water only. (Bottom) The background-free (Lorentzian line shapes), vibrational spectrum of PYP^{E46Q} derived from the $\chi^{3)}$-fit. The wavenumber positions of selected bands are presented. The parameters obtained for the respective $\chi^{(3)}$-fits are presented in Table 2.

(Table 2), but their relative intensities differ as expected when changes in the degree of resonance enhancement are made. The effect of changing the degree of resonance enhancement can be observed in the significantly different dispersive line shapes found in the PR/CARS data recorded from PYP and PYP^{E46Q} (Figure 5). Quantitative differences in resonantly enhanced CARS signal can be obtained from the value of the electronic phase factor, θ, required to accurately fit the derivative CARS signals.[20] Defined in terms of the nonlinear interaction between the radiation field (ω_1) and the electronic transition moment from which resonantly enhanced Raman scattering is generated, θ can be used to characterize the general electron distribution within a chromophore. Analogously, changes in the electron distribution within a chromophore cause not only a shift in the absorption spectrum (Figure 1), but also determine the value of θ required for an accurate $\chi^{(3)}$ fit of the derivative line shapes in the resultant CARS data (Figure 5).

The background-free, CARS spectra of PYP and PYP^{E46Q}, derived from the quantitative $\chi^{(3)}$ fits to these PR/CARS data using Lorentzian line shapes (Figure 6), consider the differences in θ values, and, therefore, the resultant Lorentzian CARS spectra contain no residual effects attributable to changing degrees of resonance enhancement. The corresponding $\chi^{(3)}$-fitting parameters (i.e., band origin position (Ω_i), bandwidth (Γ_i), and amplitudes (A_i)) for PYP and PYP^{E46Q} are presented in Table 3. The error in measuring the band position of a given vibrational feature is found typically to be <1 cm^{-1} throughout the 1100−1700 cm^{-1} region. Thus, differences in band positions of >1 cm^{-1} and measurable changes in intensities between the background-free, Lorentzian PR/CARS spectra of PYP and PYP^{E46Q} can be attributed to the effects of the Glu46/Gln

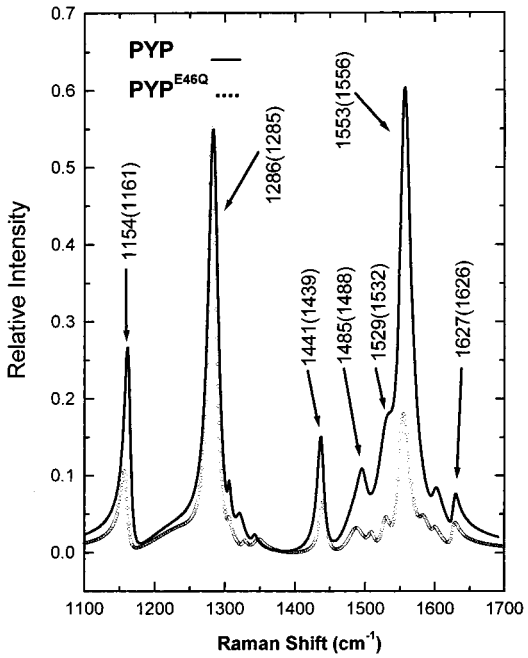

Figure 6. Background-free (Lorentzian line shapes), vibrational spectra of PYP (solid line) and PYP^{E46Q} (○ data) in the 1100−1700 cm^{-1} region. The parameters obtained for the respective $\chi^{(3)}$-fits are presented in Table 2. The wavenumber positions of selected bands are shown.

TABLE 3: Parameters (Ω_k-Band Origin Positions, Γ_k-Bandwidth (Half-Width at Half-Maximum), and A_k-Amplitudes) Derived from $\chi^{(3)}$ Fits to PR/CARS Data (ω_1 = 490 nm; 1100−1700 cm^{-1}) Assigned to PYP and PYP^{E46Q}

PYP			PYP^{E46Q}		
Ω_k (cm^{-1})	Γ_k (cm^{-1})	A_k[a]	Ω_k (cm^{-1})	Γ_k (cm^{-1})	A_k[a]
1161	5	0.65	1154	6	0.18
1243	60	0.20	1243	60	0.15
1286	8	1.00	1285	8	1.00
1306	5	0.20	1306	4	0.09
1320	9	0.18	1321	6	0.08
1343	19	0.14	1344	19	0.17
1439	4	0.49	1441	7	0.37
1447	8	0.15			
1488	18	0.30	1485	15	0.25
1505	9	0.21	1507	11	0.14
1532	16	0.40	1529	7	0.18
1556	11	1.03	1552	13	0.58
			1581	5	0.09
1597	17	0.17	1598	8	0.08
1626	7	0.16	1626	8	0.18

[a] Values for the PR/CARS amplitudes (A_k) are normalized to the amplitude of the 1286/5 cm^{-1} band.

mutation, and not to differences in θ since these have been normalized through the $\chi^{(3)}$ analysis.

The relationship between the Glu46/Gln mutation and θ can be found qualitatively in the dependence of the dispersive line shapes in CARS on θ. Since the Glu46/Gln mutation alters the hydrogen bonding to the negatively charged phenolate oxygen, the electronic distribution within the phenolate ring can be anticipated to change, thereby altering the electron density within the chromophore from which resonantly enhanced PR/CARS is generated experimentally. Quantitatively, the differences in the resultant dispersive line shapes in the PR/CARS spectra can be expressed in terms of θ: 91° for PYP and 135° for PYP^{E46Q} (for ω_1 = 490 nm and ω_s = 518−535 nm).

2. Vibrational Mode Assignments in PYP. (a) Band Intensities. One of the most prominent features in both PR/CARS spectra is the 1286/5 cm^{-1} band which is assigned to stretching vibrations delocalized over the −CC(−S−)═O skeleton (thio ester region) of the chromophore.[24] There is no significant difference (∼1 cm^{-1}) in the position of this band for PYP and PYP^{E46Q} (Figure 6, Table 2), an observation which is consistent with the assignment to normal modes involving the −CC(−S−)═O skeleton. Changes of the electron distribution within the phenolate ring are not anticipated to necessarily affect the −CC(−S−)═O vibrational modes. The same type of conclusion can be reached for the C═C stretching mode which has been assigned to the 1626 cm^{-1} band, the position of which also does not change in PYP^{E46Q} (Figure 6, Table 2).

These PR/CARS data suggest that the electron distribution within the cinnamyl chromophore is isolated into distinct regions, the phenolate ring being one region and the −CC(−S−)═O skeleton together with the C═C stretching motion being another region. This observation is consistent with the conclusion that the Glu46/Gln mutation does not directly affect the vibrational modes in the chromophore removed from the phenolate ring. The PR/CARS band intensities for PYP and PYP^{E46Q} can be related quantitatively by normalizing the respective 1286/5 cm^{-1} bands (−CC(−S−)═O skeleton, Figure 6). The same rationale suggests that the intensities of the respective 1626 cm^{-1} bands (C═C stretching) for PYP and PYP^{E46Q} should also be the same. In fact, the 1626 cm^{-1} bands appear to have slightly different intensities (1/1.05) due to the large differences in band intensities of the strong neighboring 1553/6 cm^{-1} bands (Figure 6).

(b) Phenolate/Tyrosinate Modes. Five of the remaining bands in the PR/CARS spectra of PYP and PYP^{E46Q} exhibit significant changes in both the band maxima (origin) positions and intensities (Tables 2 and 4). All of these bands are assigned to vibrational modes within the phenolate ring,[24,25] and the analysis of these changes provides insight into the influence of the Glu46/Gln mutation on the structure of separate parts of the cinnamyl chromophore, not only in its ground state but also during its photocycle, *vide infra*. The PYP vibrational bands at 1158, 1436, 1485, 1532, and 1555 cm^{-1} are assigned respectively to the Y9a, Y19b, Y19a, Y8b, and Y8a normal modes of a tyrosine-like structure.[25] Both the Y8a and Y19a modes involve an in-plane, symmetric skeleton and hydrogen stretching vibrations with different symmetric axes within the phenolate ring (Table 4). The Y8a mode has two perpendicular symmetric axes, one of which is directed along the polyene chain of the chromophore and the other is perpendicular to the polyene chain. The Y19a mode has only one symmetric axis which is directed along the polyene chain. The Y8b and Y19b modes correspond to asymmetric stretching motions (Table 4).

It is evident from the PR/CARS spectra (Figure 6) that band maxima (origin) positions for all five of these tyrosinate type bands shift with the Glu46/Gln mutation. These shifts vary from +2 to −7 cm^{-1} (ν(PYP^{E46Q}) − ν(PYP)) and are summarized together with the respective normal mode diagrams for tyrosine in Table 4. These frequency changes are larger than the ∼1 cm^{-1} accuracy of the band maxima (origin) position measurement in these PR/CARS experiments, *vide supra*. The frequencies of all the bands assigned to the phenolate ring in the PYP^{E46Q} chromophore shift (although by different degrees and in different directions) relative to the corresponding bands in PYP while the positions of the two prominent bands assigned to other parts of the PYP chromophore (1286 and 1626 cm^{-1}) remain unchanged (within experimental error).

The relative intensities of the bands assigned to modes in the phenolate ring also decrease significantly (30−50%) in PYP^{E46Q} relative to the band intensities in PYP (Figure 6, Table

TABLE 4: Tyrosine Vibrational Modes Assignable in PYP and PYP^{E46Q} to the Phenolate Ring. Band Maxima (Origin) Positions (cm^{-1}) and Shifts (δ) between PYP and PYP^{E46Q} Bands Together with Their Relative Intensities

Tyrosine Modes		Band Maxima (origin) Positions (cm^{-1})	δ(cm^{-1})	Relative Intensities
Y8a	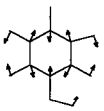	1529 (PYP ^{E46Q})	-3	0.18
		1532 (PYP)		0.40
Y8b	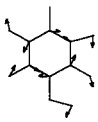	1552 (PYP ^{E46Q})	-4	0.58
		1556 (PYP)		1.03
Y9a	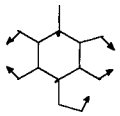	1154 (PYP ^{E46Q})	-7	0.18
		1161 (PYP)		0.65
Y19a	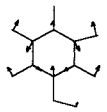	1485 (PYP ^{E46Q})	-3	0.25
		1488 (PYP)		0.30
Y19b	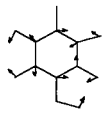	1441 (PYP ^{E46Q})	+2	0.37
		1439 (PYP)		0.49

4). These decreased intensities appear even though $\omega_1 = 460$ nm generates a stronger resonance enhancement for CARS in PYP^{E46Q} than in PYP (Figure 2). Thus, the Glu46/Gln mutation in the active site (binding pocket) of PYP alters both the positions and relative intensities of the phenolate vibrational modes.

Discussion

The strong influence of the Glu46/Gln mutation on the dynamics of the PYP photocycle is evident from the PTA data presented here. The increased rate constants (relative to those in the PYP photocycle) for the decay of I_0^{E46Q} to form $I_0^{\ddagger E46Q}$ and for the decay of $I_0^{\ddagger E46Q}$ to form I_1^{E46Q} show that both processes are influenced by the E46Q mutation and its associated alteration of the hydrogen bonding environment involving the phenolate ring oxygen in the chromophore. Since such changes in hydrogen bonding can be expected to alter the electronic charge distribution within the phenolate ring itself, it would appear that, even from the PTA data, the mechanism underlying the formation and decay of both I_0^{E46Q} and $I_0^{\ddagger E46Q}$ involve the electronic character of the phenolate ring.

The same changes in the delocalization of electronic energy within the phenolate ring observed in the kinetics (PTA) are found to influence the resonantly enhanced, vibrational spectra of PYP and PYP ^{E46Q} measured by PR/CARS. This influence appears in three different, but related, aspects of the measured PR/CARS data.

1. The frequency positions of PR/CARS band maxima (origins) assigned to specific vibrational modes within the phenolate ring are shifted by changes in the delocalized electronic energy distribution within the ring. This phenomenon is well-known whenever force constants (bond orders) differ in specific vibrational motions. Vibrational modes that do not exhibit band maxima (origin) shifts do not change their respective force constants. The observation of band shifts means explicitly that either the structure of the cinnamyl chromophore has changed or chromophore/protein interactions which can alter the delocalized electronic energy within the cinnamyl chromophore (e.g., the hydrogen bonding network) have changed.

2. The relative intensities of PR/CARS bands also depend on electronic energy distribution within the molecule. The efficiency (i.e., signal strength or cross-section) of coherent Raman scattering is a function of the electronic energy distribution. The significant reduction in the relative intensities of only those PR/CARS bands assigned previously to phenolate ring modes (cf. PYP^{E46Q} to PYP) indicates that the electronic distribution within the phenolate ring decreases in PYP^{E46Q}.

3. The influence of the Glu46/Gln mutation is also observed by changes in the electronic phase factor, θ, derived from the $\chi^{(3)}$-fitting procedure. The dependence of θ on the amino acid environment reflects differences in the electronic distribution in the phenolate ring associated with the alteration of the hydrogen bonding network (including the negatively charged oxygen, Figure 2).

It is important to note that neither the band maxima (origin) positions nor the relative intensities of any PR/CARS band not assigned to the phenolate ring change in response to the E46Q mutation. These observations suggest that the changes in electronic energy distribution found in the phenolate ring, and associated with the E46Q mutation, are generally isolated from the remainder of the PYP chromophore.

Since the PTA and PR/CARS data from PYP^{E46Q} are measured under comparable experimental conditions, their respective results can be correlated. A consideration of both the PTA (kinetic rate constants) and PR/CARS (vibrational spectra) data provide new insight into the structural properties of the PYP chromophore to be associated with the PYP and PYP^{E46Q} photocycles, and specifically with the $I_0/I_0^{\ddagger}$ and $I_0^{E46Q}/I_0^{\ddagger E46Q}$ intermediates. The PTA results show that the E46Q mutation alters the kinetics properties which connect I_0 and $I_0^{\ddagger}$ (I_0^{E46Q} and $I_0^{\ddagger E46Q}$), while the PR/CARS data show that the E46Q mutation specifically alters the vibrational structure only in the phenolate ring of the PYP chromophore. In both cases, the changes are attributable to differences in either the chromophore structure and/or the electronic distribution within the phenolate ring. No other part of the PYP cinnamyl chromophore appears to be altered by the E46Q mutation. Thus, a consideration of these two observations together suggests that the structural changes in I_0 and $I_0^{\ddagger}$ (I_0^{E46Q} and $I_0^{\ddagger E46Q}$) involve primarily the phenolate ring. The role of structural changes in the remainder of the cinnamyl chromophore in the formation of I_0 and $I_0^{\ddagger}$ (I_0^{E46Q} and $I_0^{\ddagger E46Q}$), including the C═C isomerization, is as yet unclear. If C═C isomerization is involved in the formation and decay of the I_0 and $I_0^{\ddagger}$ (I_0^{E46Q} and $I_0^{\ddagger E46Q}$), it has yet to be experimentally observed in the vibrational spectra of the ground state.

This conclusion does not indicate that C═C isomerization is absent from all stages of the PYP (PYP^{E46Q}) photocycle but rather that it occurs after the formation of $I_0^{\ddagger}$ ($I_0^{\ddagger E46Q}$). These results do suggest that other structural changes in the cinnamyl chromophore occur before C═C isomerization in the PYP (PYP^{E46Q}) photocycle. Thus, the characterization of C═C isomerization as the primary structural event in the PYP photocycle[9] requires reconsideration. Time-resolved CARS

spectra measured directly from the I_0 and $I_0^{\ddagger}$ (I_0^{E46Q} and $I_0^{\ddagger E46Q}$) intermediates would directly address these issues.

Acknowledgment. This work was supported financially by an NSF Grant (MCB 9722781). The authors wish to acknowledge the technical assistance of J. Fitch in the preparation of the PYP and PYP^{E46Q} samples. L.U. also wishes to gratefully acknowledge financial support from Innovative Lasers Corp.

References and Notes

(1) Meyer, T. E.; Tollin, G.; Causgrove, T. P.; Cheng, P.; Blankenship, R. E. *Biophys. J.* **1991**, *59*, 988.

(2) Chosrowjan, H.; Mataga, N.; Nakashima, N.; Imamoto, Y.; Tokunaga, F. *Chem. Phys. Lett.* **1997**, *270*, 267.

(3) Ujj, L.; Devanathan, S.; Meyer, T. E.; Cusanovich, M. A.; Tollin, G.; Atkinson, G. H. *Biophys. J.* **1998**, *75*, 406.

(4) Sprenger, W. W.; Hoff, W. D.; Armitage, J. P.; Hellingwerf, K. J. *J. Bacteriol.* **1993**, *175*, 3096.

(5) Jiang, Z. Y.; Swem, L. R.; Rushing, B. G.; Devanathan, S.; Tollin, G.; Bauer, C. E. *Science* **1999**, *285*, 406

(6) Hoff, W. D.; Dux, P.; Hard, K.; Devreese, B.; Nugterenroodzant, I. M.; Crielaard, W.; Boelens, R.; Kaptein, R.; Vanbeeumen, J.; Hellingwerf, K. F. *Biochemistry* **1994**, *33*, 13959

(7) Baca, M.; Borgstahl, G. E. O.; Boissinot, M.; Burke, P. M.; Williams, D. R.; Slater, K. A.; Getzoff, E. D. *Biochemistry* **1994**, *33*, 14369.

(8) Borgstahl, G. E. O.; Williams, D. R.; Getzoff, E. D. *Biochemistry* **1995**, *34*, 6278.

(9) Genick, U. K.; Borgstahl, G. E. O.; Ng, K.; Ren, Z.; Pradervand, C.; Burke, P. M.; Srajer, V.; Teng, T. Y.; Schildkamp, W.; McRee, D. E.; Moffat, K.; Getzoff, E. D. *Science* **1997**, *275*, 1471

(10) Perman, B.; Srajer, V.; Ren, Z.; Teng, T. Y.; Pradervand, C.; Ursby, T.; Bourgeois, D. Schotte, F.; Wulff, M.; Kort, R.; Hellingwerf, K.; Moffat, K. *Science* **1998**, *279*, 1946

(11) Genick, U. K.; Soltis, S. M.; Kuhn, P.; Canestrelli, I. L.; Getzoff, E. D. *Nature* **1998**, *392*, 206.

(12) Xie, A. H.; Hoff, W. D.; Kroon, A. R.; Hellingwerf, K. J. *Biochemistry* **1996**, *35*, 14671

(13) Demchuk, E.; Genick, U. K.; Woo, T. T.; Getzoff, E. D.; Bashford, D. *Biochemistry* **2000**, *39*, 1100

(14) Hoff, W. D.; Van Stokkum, I. H. M.; Gural, J.; Hellingwerf, K. J. *Biochim. Biophys. Acta* **1997**, *1322*, 151

(15) Genick, U. K.; Devanathan, S.; Meyer, T. E.; Canestrelli, I. L.; Williams, E.; Cusanovich, M. A.; Tollin, G.; Getzoff, E. D. *Biochemistry* **1997**, *36*, 8.

(16) Meyer, T. E.; Yakali, E.; Cusanovich, M. A.; Tollin, G. *Biochemistry* **1987**, *26*, 418

(17) Hoff, W. D.; Van Stokkum, I. H. M.; Van Ramesdonk, H. J.; Van Brederode, M. E.; Brouwer, A. M.; Fitch, J. C.; Meyer, T. E.; Van Grondelle, R.; Hellingwerf, K. J. *Biophys. J.* **1994**, *67*, 1691

(18) Meyer, T. E. *Biochim. Biophys. Acta* **1985**, *806*, 175.

(19) Ujj, L.; Jager, F.; Atkinson, G. H. *Biophys. J.* **1998**, *74*, 1492.

(20) Devanathan, S.; Lin, S.; Cusanovich, M. A.; Woodbury, N.; Tollin, G. *Biophys. J.* **2000**, *79*, 2132.

(21) Ujj, L.; Zhou, Y. D.; Sheves, M.; Ottolenghi, M.; Ruhman, S.; Atkinson, G. H. *J. Am. Chem. Soc.* **2000**, *122*, 96.

(22) Zhou, Y. D.; Ujj, L.; Lou, J. H.; Jager, F.; Nakanishi, K.; Atkinson, G. H. *J. Mol. Struct.* **1999**, *478*, 107.

(23) Jäger, F.; Ujj, L.; Atkinson, G. H. *J. Am. Chem. Soc.* **1997**, *119*, 12610.

(24) Kim, M.; Mathies, R. A.; Hoff, W. D.; Hellingwerf, K. J. *Biochemistry* **1995**, *34*, 12669.

(25) Harada, I.; Takeuchi, H. *Spectroscopy of Biological Systems*; John Wiley & Sons: Chichester, U.K., 1996; Vol. 13, Chapter 3.